Voltage-Stability-Guided Two-Stage Restoration Strategy for Power Systems with Embedded VSC-HVDC

Xingyu Liu,Yiheng Bian*,Sibo Wang,Gengfeng Li
State Key Laboratory of Electrical Insulation and Power Equipment
Xi'an Jiaotong University
Xi'an, China
liuxingy@stu.xjtu.edu.cn,byh0xyz@mail.xjtu.edu.cn,3225974469@qq.com,gengfengli@xjtu.edu.cn

***Abstract*—With the rising presence of inverter-based generators (IBGs) and embedded voltage source converter-based high-voltage direct current (VSC-HVDC) links, modern power systems face new black start challenges, as traditional strategies designed for synchronous generator-dominated grids are inadequate. Existing studies often overlook the critical distinction between grid-following (GFL) and grid-forming (GFM) IBGs, potentially misidentifying GFL which are vulnerable to voltage instability in weak grids—as reliable black start sources. Furthermore, coordinated restoration methods for AC/DC hybrid systems are underdeveloped. To address these gaps, a two-stage sequential restoration framework is proposed: Stage I uses a mixed-integer second-order cone program to optimize unit commitment and load pickup, excluding complex voltage constraints due to its nonlinearity; Stage II then verifies the voltage stability of GFL, iteratively refining the Strategy by enforcing active power limits if instability is detected. Validated on a modified IEEE 39-bus system, the framework demonstrates that GFM and VSC-HVDC accelerate restoration, while the two-stage approach effectively prevents voltage collapse caused by GFL integration with high computational efficiency.**

***Index Terms*—extreme events, resiliency, embedded VSC-HVDC, static voltage stability, inverter-based generator**

I. Introduction

In recent years, extreme events have become increasingly frequent, highlighting the critical importance of building resilient power systems. As the new power system continues to evolve [1], the development of innovative restoration strategies has become an urgent research priority.

The increasing penetration of IBGs, primarily GFL types, is displacing conventional synchronous generators (SGs). Due to their inherent lack of inertia, the voltage stability of GFL, especially under the weak grid conditions typical of initial restoration, must be rigorously assessed to prevent voltage collapse [2]. Concurrently, the integration of GFM IBGs, often using virtual synchronous generator (VSG) control, is enhancing system strength and actively establishing voltage references, which accelerates restoration [3]. Existing studies [4], [5], [6] , however, frequently fail to distinguish between GFL and GFM types, leading to the restoration strategy inapplicable to the IBG in the real grids. And no consideration was given to the GFL's voltage stability and GFM's voltage support capability during the restoration period.

Moreover, the grid structure itself is also undergoing transformation. The traditional pure AC grid is transforming into an AC/DC hybrid grid with embedded VSC-HVDC links [8]. These links not only offer expanded restoration pathways but also use their converter stations to bolster system strength and stability. However, the existing studies did not take this into account. Therefore, for transmission systems that incorporate IBG and VSC-HVDC, developing resilient restoration strategies that are suitable for their characteristics has become a core issue for ensuring the safe and efficient restoration of modern power systems.

This paper proposes a sequential black start restoration strategy for AC/DC hybrid transmission grids that incorporate embedded VSC-HVDC links and IBGs. The main innovative contributions are as follows:

1) This paper distinguishes the functions and characteristics of GFM and GFL during the restoration process, models the embedded VSC-HVDC system, establishes a voltage stability criterion for GFL buses based on the SDSCR, and proposes a black-start strategy that takes into account time-varying topology and sequential unit restoration mechanisms.
2) To effectively incorporate the nonlinear voltage stability constraints into the optimization strategy, this paper adopts an Optimize-and-Verify approach and establishes a two-stage model. In Stage I, the optimization is carried out without considering the voltage stability constraints. After obtaining an initial solution, the voltage stability of the GFL units is verified. If the verification fails, the corresponding infeasibility constraints are introduced, and the unit commitment, transmission line, and bus energized results obtained from Stage I are fixed. A fast re-optimization is then performed in Stage II to obtain a secure and feasible solution.

II. Modeling of Power System Restoration

A typical structure of a new regional transmission system, which includes IBGs and an embedded P2P VSC-HVDC link, is illustrated in Fig. 1. In the following sections, we will first introduce the objective function and the constraints.

A. Objective Function

The proposed model aims to minimize the total cost during the restoration process. This total cost comprises the startup cost of generation units, the no-load operating cost of units, the unit generation cost, and the penalty cost associated with load shedding.

Supported by Smart Grid National Science and Technology Major Project under Grant 2024ZD0801200.

979-8-3315-8138-1

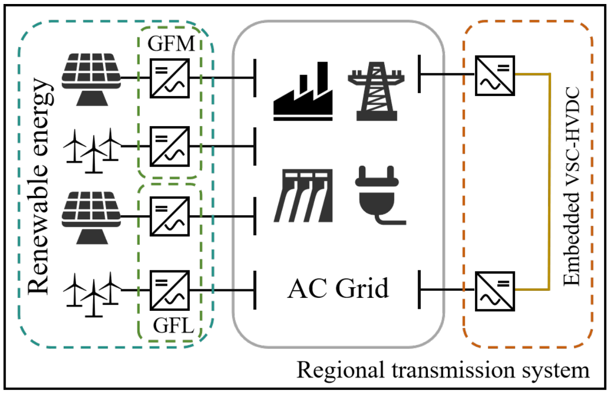

Fig. 1: Regional transmission system.

$$\min \ obj = \sum_{t\in\mathcal{T}}\sum_{g\in\mathcal{G}} (\delta_{g,t} - \delta_{g,t-1}) C_g^{SU} + \sum_{t\in\mathcal{T}}\sum_{g\in\mathcal{G}} \delta_{g,t} C_g^{NL} \Delta t + \sum_{t\in\mathcal{T}}\sum_{g\in\mathcal{G}} P_{g,t}^G C_g^{OP} \Delta t + \sum_{t\in\mathcal{T}}\sum_{i\in\mathcal{I}} \left(P_{i,t}^{D,\max} - P_{i,t}^D\right) C_i^{LD} \Delta t \quad (1)$$

Where, C_g^{SU},C_g^{NL} andC_g^{OP} denote the start-up, no-load, and operating costs of unit g; C_i^{LD} the load curtailment penalty at bus i; Δt the time step duration; $\delta_{g,t}$ the commitment status and $P_{g,t}^G$ the active power output of unit g; and $P_{i,t}^D$ (with maximum $P_{i,t}^{D,\max}$) the active load at bus$i$.

B. Generator Model

Considering the start-up and ramping processes of the generating units, the resulting dynamic operating constraints are formulated as follows [7]:

$$0 \le P_{g,\tau}^G \le \overline{P_g}\delta_{g,t}, \quad t \le \tau \le t + T_g^{CR} \quad (2)$$

$$\underline{P_g}\delta_{g,t} \le P_{g,\tau}^G, \quad \tau \ge t + T_g^{CR} + \left(\underline{P_g}/R_g^{\max}\right) \quad (3)$$

$$-R_g^{\max}\Delta t \le P_{g,t-1}^G - P_{g,t}^G \le R_g^{\max}\Delta t \quad (4)$$

Where, $\overline{P_g} = P_{g,\max}^G + P_g^{CR}$, $\underline{P_g} = P_{g,\min}^G + P_g^{CR}$. $R_g^{\max}$ is the maximum ramping rate of unit g. T_g^{CR} is the cold start-up time of unit g. The following constraints define the reactive power capability limits of the generators:

$$Q_{g,t}^G = 0, \quad t < T_g^{CR} \quad (5)$$

$$Q_g^{G,\min}\delta_{g,t-T_g^{CR}} \le Q_{g,t}^G \le Q_g^{G,\max}\delta_{g,t-T_g^{CR}}, \quad t \ge T_g^{CR} \quad (6)$$

where, $Q_g^{G,\min}$ and $Q_g^{G,\max}$ are the minimum and maximum reactive power outputs of unit g, respectively. This constraint enforces the requirement that reactive power support can only be provided when the unit is delivering active power.

C. AC Network Flow Constraints

The power flow constraints of the electrical system are modeled using a linearized AC power flow formulation. The constraints are given as follows:

$$P_{ij,t} = [g_{ij}(V_{i,t} - V_{j,t}) - b_{ij}(\theta_{i,t} - \theta_{j,t})]\delta_{ij,t} \quad (7)$$

$$Q_{ij,t} = [-b_{ij}(V_{i,t} - V_{j,t}) - g_{ij}(\theta_{i,t} - \theta_{j,t})]\delta_{ij,t} \quad (8)$$

where, $P_{ij,t}$ and $Q_{ij,t}$ are the active and reactive power flows on line ij; g_{ij} and b_{ij} are its conductance and susceptance; $V_{i,t}$ and $\theta_{i,t}$ are the voltage magnitude and phase angle at bus i; and $\delta_{ij,t}$ indicates whether line ij is active. Although the original formulation contains bilinear terms, they can be readily linearized for computational efficiency.

$$P_{g,t}^G - P_g^{CR}\delta_{g,t} + P_{iv,t}^{IV} - P_{i,t}^D - P_{c,t}^{cv,ac} = \sum_{j\in\pi(i)} P_{ij,t}, \quad (9)$$

$$Q_{i,t}^G + Q_{iv,t}^{IV} - Q_{i,t}^D - Q_{i,t}^{cv,ac} = \sum_{j\in\pi(i)} Q_{ij,t}, \quad (10)$$

where, $\pi(i)$ is the set of all transmission lines connected to bus i. $P_{c,t}^{cv,ac}$ and $Q_{c,t}^{cv,ac}$ are the active and reactive power injected into AC side of converter c. $P_{iv,t}^{IV}$ and $Q_{iv,t}^{IV}$ are the active and reactive power injected by RE inverter iv. $P_{i,t}^D$ and $Q_{i,t}^D$ are the active and reactive loads at bus i.

The bus voltage magnitudes and phase angles must satisfy the following safety constraints:

$$V_{\min,i} \le V_{i,t} \le V_{\max,i} \quad (11)$$

$$P_{ij,t}^2 + Q_{ij,t}^2 \le S_{\max,ij}^2, \quad (12)$$

D. VSC-HVDC Constraints

Considering only P2P embedded VSC-HVDC links, each HVDC link consists of two VSCs connected to different AC buses. The converter losses cannot be ignored, which are represented by a linear relationship [9]:

$$P_{c,t}^{cv,loss} = a_c^{cv} + b_c^{cv}|P_{c,t}^{cv,ac}| \quad (13)$$

$$P_{c,t}^{cv,ac} + P_{c,t}^{cv,dc} = P_{c,t}^{cv,loss} \quad (14)$$

where, $P_{c,t}^{cv,loss}$ is the total power loss of converter c. a_c^{cv} and b_c^{cv} are the fixed and variable loss coefficients for converter c, respectively. $P_{c,t}^{cv,dc}$ is the DC-side active power of converter c. The convention adopted is that the power flow direction is positive when power flows into the converter from the grid.

To linearize the absolute value term within the equation, an auxiliary binary variable, $\delta_{c,t}^{dir}$, is introduced to indicate whether converter c is operating as a rectifier or an inverter, which can indicate the positive or negative nature of the variable $P_{c,t}^{cv,ac}$.

$$P_{c,t}^{cv,ac} \ge P_c^{cv,ac,\min}\left(1 - \delta_{c,t}^{dir}\right) \quad (15)$$

$$P_{cv,ac}^{c,t} \le \varepsilon + P_c^{cv,ac,\max}\delta_{c,t}^{dir} \quad (16)$$

Where, ε is a very small number. By using auxiliary variables $\delta_{c,t}^{dir}$, then it is easy to linearize the constraints containing absolute values.

$$P_c^{cv,dc,\min} \le P_{c,t}^{cv,dc} \le P_c^{cv,dc,\max} \quad (17)$$

$$P_c^{cv,ac,\min} \le P_{c,t}^{cv,ac} \le P_c^{cv,ac,\max} \quad (18)$$

$$Q_c^{cv,ac,\min} \le Q_{c,t}^{cv,ac} \le Q_c^{cv,ac,\max} \quad (19)$$

$$(P_{c,t}^{cv,ac})^2 + (Q_{c,t}^{cv,ac})^2 \le (S_c^{cv,ac,\max})^2\delta_{c,t} \quad (20)$$

979-8-3315-8138-1

Due to the decoupled control capability of the VSC, the active and reactive power injections can be controlled independently. the active and reactive power injection constraints for the converter are presented as above. The HVDC link power flow is modeled using a linearized power flow approach, where DC-side losses are neglected:

$$P^{cv,dc}_{c_1,t} + P^{cv,dc}_{c_2,t} = 0 \tag{21}$$

where c_1 and c_2 denote the two converters of one VSC-HVDC link.

E. Load Restoration Constraints

The following constraints govern the process of load restoration across the system:

$$0 \le P^D_{i,t} \le P^{D,\max}_{i,t} \delta_{i,t} \tag{22}$$

$$P^D_{i,t} \ge P^D_{i,t-1} \tag{23}$$

$$Q^D_{i,t} = P^D_{i,t} \cdot \tan \varphi^D_i \tag{24}$$

where, φ^D_i is the load power factor angle at bus i. This formulation ensures that restored load never exceeds its maximum demand, increases monotonically over time, and restores reactive load in fixed proportion to active load according to a constant power factor.

F. IBG Constraints

IBGs can be classified into two types: GFM & GFL. The GFM can actively establish the voltage, whereas the GFL can only operate by following the grid voltage. Consequently, GFL can only be connected to the grid after their connection bus has been activated, while GFM are not subject to this restriction and can serve as black start power sources. For GFM, the relevant constraints are formulated as follows:

$$0 \le P^{IV}_{iv,t} \le P^{IV,\max}_{iv,t} \tag{25}$$

$$(P^{IV}_{iv,t})^2 + (Q^{IV}_{iv,t})^2 \le (S^{IV,\max}_{iv})^2 \tag{26}$$

where, $P^{IV,\max}_{iv,t}$ is the maximum active power output of RE inverter iv. $S^{IV,\max}_{iv}$ is its rated apparent power. For GFL inverters, the constraints are formulated as follows:

$$0 \le P^{IV}_{iv,t} \le P^{IV,\max}_{iv,t} \cdot \delta_{i,t-1} \tag{27}$$

$$(P^{IV}_{iv,t})^2 + (Q^{IV}_{iv,t})^2 \le (S^{IV,\max}_{iv})^2 \cdot \delta_{i,t-1} \tag{28}$$

G. Connectivity of Energized Grid

To ensure the integrity of the activated status of buses and lines during the restoration process, and to guarantee the connectivity of the energized grid, the constraints are formulated as follows [11]:

$$\delta_{i,t} \ge \delta_{g,t} \tag{29}$$

$$\begin{cases} \delta_{ij,t} \le \delta_{i,t} \\ \delta_{ij,t} \le \delta_{j,t} \end{cases} \tag{30}$$

$$\delta_{ij,t} \le \delta_{i,t-1} + \delta_{j,t-1} \tag{31}$$

(29) ensures that a generating unit's start-up is contingent upon the simultaneous activation of its connection bus. (30) ensures that a transmission line can only be activated if both of its connected buses are also activated. (31) ensures that a line can only connect buses that were already activated in the previous time step.

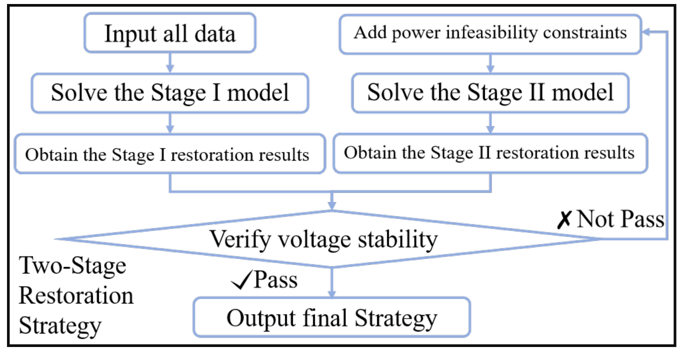

Fig. 2: Two-Stage restoration strategy flowchart.

$$\begin{cases} \delta_{dcl,t} \le \delta_{i,t} \\ \delta_{dcl,t} \le \delta_{j,t} \end{cases} \tag{32}$$

$$\delta_{dcl,t} \le \delta_{i,t-1} + \delta_{j,t-1} \tag{33}$$

$$\delta_{i,t} \le \sum_{j \in \pi(i)} \delta_{ij,t} + \delta_{dcl,t} \tag{34}$$

These represents the activation of the VSC-HVDC link, where a single binary variable simultaneously controls the operational status of the HVDC line and its two converters. Buses i and j denote the AC network nodes to which the two respective converters are connected. (34) ensures that the activation of any bus must be contingent upon its connection to at least one activated transmission line or one activated VSC-HVDC link.

$$\begin{cases} \delta_{i,t} \ge \delta_{i,t-1} \\ \delta_{ij,t} \ge \delta_{ij,t-1} \\ \delta_{g,t} \ge \delta_{g,t-1} \end{cases} \tag{35}$$

(35) represents the temporal continuity of the activated status for buses, lines, and generating units: once activated, they must remain active in all subsequent time steps. The VSC-HVDC link's activation status is not subject to this persistence constraint, given its ability to perform fast start-up and shutdown operations.

III. Two-Stage Power System Restoration Model

The restoration strategy is executed via a two-stage power system restoration model. In the Stage I, the model is solved without considering voltage stability constraints. Upon successful completion of Stage I, the results are subjected to a voltage stability verification. If the solution passes the verification, the results are outputted.

If the verification fails, the activated statuses of lines, generating units, and buses are fixed. The infeasible constraints derived during the verification process are added to the formulation of Stage II, which is then quickly solved to yield the final restoration plan.The overall procedure is illustrated in the flowchart shown in Fig. 2.

A. Stage I Model

The Stage I restoration model is formulated as a Mixed-Integer Second-Order Cone Program (MISOCP), with its

979-8-3315-8138-1

complete objective function and all associated constraints fully specified in Section II.

$$\min obj(1)$$
$$\text{s.t.}(2) - (35)$$

Upon the successful solution of the Stage I problem, the resulting optimal solution is recorded, and the process proceeds to the voltage stability verification step.

B. Voltage Stability Verification for GFL

As GFL inverters lack inertial support and rely on grid voltage reference, their voltage stability is critical to avoid collapse during the weak-grid stage of restoration. The stability criterion adopted in this paper is based on the SDSCR.

Voltage stability of GFL inverters is determined by the system's ability to maintain voltage at their connected buses under power injection changes. Research [12] shows that the critical stability boundary occurs when the equivalent active-reactive power jacobian matrix J of the IBG loses rank, indicating that small perturbations in power injection will cause unbounded voltage deviations. By solving for $|J| = 0$ and subsequent simplification, the following quadratic voltage stability criterion is obtained:

$$\hat{P}_{iv}^2 + \hat{Q}_{iv}^2 \leq \left(\hat{Q}_{iv} + \Gamma_{iv} - \varepsilon_{iv}\right)^2 \tag{36}$$

where, $\hat{P}_{iv}$ and $\hat{Q}_{iv}$ are the equivalent active and reactive power injections of the IBG, respectively. ε_{iv} denotes a stability margin, introduced to enhance robustness. Γ_{iv} is a constant related to the system parameters. The calculation formula is given by:

$$\hat{P}_{iv} = P_{iv} + \sum_{iv' \in IV, iv' \neq iv} \frac{|Z_{\Phi(iv)\Phi(iv')}|}{|Z_{\Phi(iv)\Phi(iv)}|} P_{iv'} \tag{37}$$

$$\hat{Q}_{iv} = Q_{iv} + \sum_{iv' \in IV, iv' \neq iv} \frac{|Z_{\Phi(iv)\Phi(iv')}|}{|Z_{\Phi(iv)\Phi(iv)}|} Q_{iv'} \tag{38}$$

$$\Gamma_{iv} = \frac{1}{2|Z_{\Phi(iv)\Phi(iv)}|} \tag{39}$$

where $\Phi(iv)$ represents the bus of the system where inverter iv is connected. To determine the system impedance values, $Z_{\Phi(iv)\Phi(iv)}$ and $Z_{\Phi(iv)\Phi(iv')}$, we first introduce the system admittance matrix, Y:

$$\mathbf{Y} = \mathbf{Y}^0 + \mathbf{Y}^{SG} + \mathbf{Y}^{VSG} \tag{40}$$

$$Y_{ii}^{SG} = \frac{1}{X_g^{SG}} \cdot \delta_{g,t} \quad i = G(g) \tag{41}$$

$$Y_{ii}^{VSG} = \frac{1}{X_{iv}^{VSG}} \cdot \alpha_{iv,t} \quad i = \Phi(iv) \tag{42}$$

where, $\mathbf{Y}^0$ is the base system admittance matrix. $\mathbf{Y}^{SG}$ is the admittance increment matrix due to SGs. $\mathbf{Y}^{VSG}$ is the admittance increment matrix due to VSGs. X_g^{SG} is the synchronous reactance of unit g. X_{iv}^{VSG} is the equivalent virtual synchronous reactance of inverter iv. $\alpha_{iv,t}$ represents the percentage of available capacity at time t. It should be noted that the inverter station of the VSC-HVDC link can also adopt VSG, allowing it to contribute the equivalent virtual synchronous reactance, X_c^{VSG} [10]. All other undefined entries in the increment matrices are zero.

By inverting the system admittance matrix, Y, the system impedance matrix $Z = Y^{-1}$ is obtained, which is then used to calculate the voltage stability index for every GFL. If the voltage stability criterion is satisfied by all GFL at every point of connection throughout the entire restoration process, the restoration plan is deemed feasible, and the Stage I results are outputted directly. Otherwise, the process proceeds to the Stage II model.

C. Stage II Model

Based on the voltage stability calculation formula, an increase in active power, when the system topology remains unchanged, tends to lead to voltage instability. Consequently, guaranteeing voltage stability can be achieved by constraining the upper limit of the active power. Following the voltage stability verification results, the set of time instances where IBG iv fails the stability criterion, denoted as T_{fail}, is recorded. The upper limit of its active power injection, $\overline{P}_{iv,t}^{IV}$, is then calculated using the Stage I results as follows: $\overline{P}_{iv,t}^{IV} = [(\hat{Q}_{iv} + \Gamma_{iv} - \varepsilon_{iv})^2 - \hat{Q}_{iv}^2]^{\frac{1}{2}}$. The following constraint is then added to the Stage II model formulation:

$$\overline{P}_{iv,t}^{IV} \leq P_{iv,t}^{IV} \quad \forall iv \in IV_{follow}, t \in T_{fail} \tag{43}$$

Given the high computational complexity and time-consuming nature of large-scale mixed-integer programming, to promptly derive a feasible restoration strategy, the Stage II removes the energized grid connectivity constraints and fixing

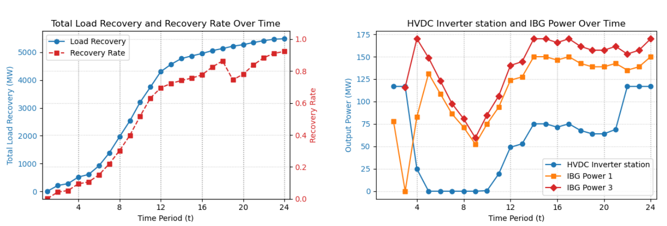

(a) Load recovery rate and restored power (b) HVDC inverter station and IBG power

Fig. 3: Results of the case study.

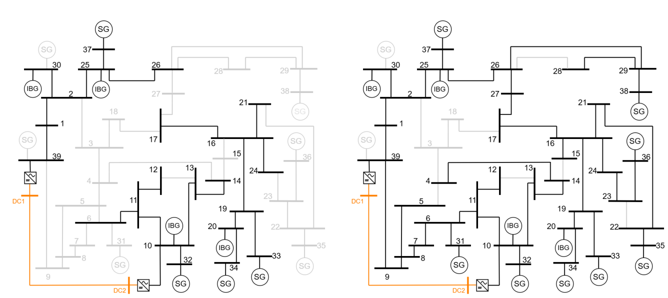

(a) t=3 (b) t=10

Fig. 4: Energized system status.

979-8-3315-8138-1

TABLE I: Summary of Voltage Instability Analysis and Constraints in Different Stages

Stage No.	Execution Time	Voltage Instability Points	Constraints Added to the Next Iteration
Stage I	691 s	IBG 1: $t = 2, 4$; IBG 3: $t = 3$	$\overline{P}_{1,2}^{IV} = 83.2, \overline{P}_{1,4}^{IV} = 83.59, \overline{P}_{3,3}^{IV} = 116.11$
Stage II-1	0.81 s	IBG 1: $t = 2$	$\overline{P}_{1,2}^{IV} = 78.4$
Stage II-2	0.83 s	None	None

the activation statuses of all lines $\delta_{ij,t}, \delta_{dcl,t}$, generating units $\delta_{g,t}$, and buses $\delta_{i,t}$.

Once the Stage II model is solved, the resulting solution is subjected to the voltage stability verification once again. If the solution passes the criterion, the final results are outputted. If it fails, constraints are added using the same methodology until the verification is successfully passed.

IV. Case Study

The proposed approach is tested on a modified IEEE 39-bus system. The test system is augmented by adding four IBG units and one VSC-HVDC link to simulate post-event restoration. GFL IBG 1 and IBG 3 are connected to the 10 and 20 bus, with the upper limits of active power being 150 and 170 MW respectively. A total of eight available generators are considered in the system. To simulate the dynamic changes in load and renewable generation, a distinct load demand and RE output are set for each time step. The SGs on bus 30 and bus 39 cannot start due to the event.

Upon the successful solution of the Stage I model, the system's activation statuses were obtained and subsequently subjected to a voltage stability verification. Stage I shows that IBG 1 started at time 2 and IBG 3 started at time 3. Based on these critical verification results, the upper limits of active power injection for these instability IBGs were calculated accordingly to rectify the infeasibility. As shown in Table I, these constraints were then incorporated into the Stage II model for re-solution.

After two iterations, ultimately a final restoration strategy that successfully passed the voltage stability verification was obtained. It can be seen that if no voltage check is conducted, GFL will cause a voltage collapse when it is just started and connected to the grid. By decomposing the problem and fixing the binary variables, the iterative process of the second stage achieves high computational efficiency, despite the prolonged solution time of the first stage.

Fig. 3a shows the system restoration rate and the total restored load, the introduction of GFM and the VSC-HVDC link effectively enhances both the speed and the quantity of system restoration. Furthermore, the GFL also contribute to the improved system restoration capability after their successful connection and start-up.

The power injections of the VSC-HVDC link and the GFL are in Fig. 3b. The VSC-HVDC takes on a critical active power transmission responsibility in the early and late stages of restoration process. The energized status of the grid topology is shown in Fig. 4. It can be clearly seen that black start power sources and GFM are started first, followed by the gradual energization of other components. Notably, the VSC-HVDC link is strategically energized at critical moments during the restoration.

A sensitivity analysis of the impedance is conducted, considering measurement errors. The synchronous reactance of both the SG and the VSG is perturbed by 10%. Owing to the existence of the stability margin, no false negatives occur in the stability assessment, thereby ensuring the robustness of the model.

V. Conclusion and Future Work

This paper proposes a two-stage framework for power system restoration in grids with high IBG and VSC-HVDC penetration. It addresses voltage instability risks posed by GFL during black-start by first determining a feasible restoration sequence, then enforcing voltage stability via iterative verification. Tests on a modified IEEE 39-bus system show that coordinating GFM and VSC-HVDC enhances restoration speed and resilience, effectively balancing computational efficiency with dynamic stability requirements.

In future work, we will consider other stability aspects of GFL converters, such as deriving additional stability criteria based on the generalized short-circuit ratio. We will investigate the communication and control challenges associated with the practical deployment of the proposed strategy.

References

[1] Wang, Q. H., Huang, Y. J., Zhu, Y. K., Liu, J. Z., and Du, Z. M., "Development direction, technical issues, and key construction tasks for new power system," *Renewable Energy System and Equipment*, vol. 1, no. 1, Pages 1-7, 2025.

[2] A. R. Nageswa Rao, P. Vijaya, and M. Kowsalya, "Voltage stability indices for stability assessment: A review," *Int. J. Ambient Energy*, vol. 42, no. 7, pp. 829–845, 2021.

[3] Z. Pan, N. Jenkins, and J. Wu, "Black start from renewable energy resources: Review and a case study of Great Britain," *Renew. Sustain. Energy Rev.*, vol. 209, p. 115143, 2025.

[4] F. Qiu, Y. Zhang, R. Yao, and P. Du, "Power system restoration with renewable participation," *IEEE Trans. Sustain. Energy*, vol. 14, no. 2, pp. 1112–1121, Apr. 2023.

[5] L. Jiang, Z. Bie, T. Long, X. Wang, H. Xie, and G. Li, "A post-event generator start-up strategy for renewable penetrated transmission system considering dynamic frequency regulation," *IEEE Trans. Sustain. Energy*, vol. 14, no. 2, pp. 1135–1150, Apr. 2023.

[6] L. Sun, Y. Wei, Z. Lin, X. Yang, M. Li, F. Wen, and M. Ding, "Determining optimal generator start-up sequence in bulk power system restoration considering uncertainties: A confidence gap decision theory based robust optimization approach," *Int. J. Electr. Power Energy Syst.*, vol. 153, p. 109365, 2023.

[7] G. Patsakis, D. Rajan, I. Aravena, J. Rios, and S. Oren, "Optimal black start allocation for power system restoration," *IEEE Trans. Power Syst.*, vol. 33, no. 6, pp. 6766–6776, Nov. 2018.

[8] C. Hu, X. Wu, and H. Cai, "Research on the operation performance enhancement of hybrid AC/DC power system with multi-type embedded HVDC," *IEEE Trans. Power Del.*, vol. 40, no. 1, pp. 606–617, Feb. 2025.

[9] H. Ergun, J. Dave, D. Van Hertem, and F. Geth, "Optimal power flow for AC–DC grids: Formulation, convex relaxation, linear approximation, and implementation," *IEEE Trans. Power Syst.*, vol. 34, no. 4, pp. 2980–2990, Jul. 2019.

[10] A. E. Leon and J. M. Mauricio, "Virtual synchronous generator for VSC-HVDC stations with DC voltage control," *IEEE Trans. Power Syst.*, vol. 38, no. 1, pp. 728–738, Jan. 2023.

[11] Y. Xie, D. Li, Y. Xu, Q. Wu, and M. Yin, "A MILP-based restoration planning method for generator start-up considering flexible re-energizing times of transmission lines," *Int. J. Electr. Power Energy Syst.*, vol. 124, p. 106357, 2021.

[12] Z. Chu and F. Teng, "Voltage stability constrained unit commitment in power systems with high penetration of inverter-based generators," *IEEE Trans. Power Syst.*, vol. 38, no. 2, pp. 1572–1582, Mar. 2023.

979-8-3315-8138-1